Electronic supplementary information

A high precision MUA-spaced single-cell sensor for cellular receptor assay based on bifunctional Au@Cu-PbCQDs nanoprobes

Dongping Long[#], Chengchi Chen[#], Chenyu Cui, Zheng Yao and Peihui Yang*

Department of Chemistry, Jinan University, Guangzhou 510632, China.

E-mail: typh@jnu.edu.cn; Tel/Fax: +86-20-85223039

S1.1 UV–vis spectra of Au@Cu-PbCQDs nanoprobes

The fabrication of Au@Cu-PbCQDs nanoprobes was demonstrated by UV-vis absorbance spectra. As shown in Fig. S1, compared with the spectrum of AuNPs (Fig. S1A), the L-cysteine-modified AuNPs exhibited a new absorption band at 700 nm, which was attributed to L-cysteine modification. The absorption peak of Au@Cu nanoparticles was redshifted correspondingly, because Cu^{2+} was connected to the L-cysteine-modified AuNPs. Moreover, compared with the CQDs, the PbCQDs exhibited a large absorption at 280 nm, which was due to the π-π* transition of the C=C bonds. The Au@Cu-PbCQDs nanoprobes (Fig. S1B) had Au@Cu nanoparticles and PbCQDs the absorption bands, indicating that the Au@Cu-PbCQDs nanoprobes was successfully fabricated.

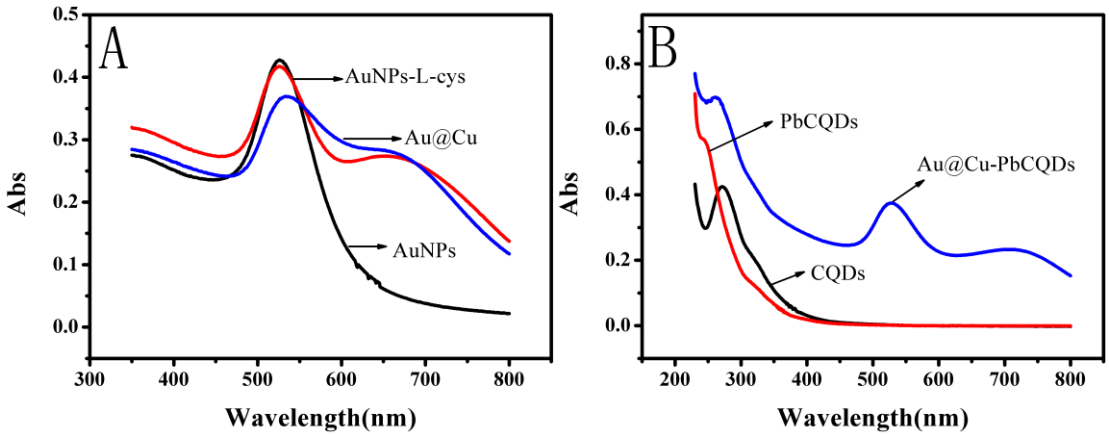

Fig. S1 UV–vis spectra of (A) Au@Cu; (B) Au@Cu-PbCQDs nanoprobes.

S1.2 Characterization of single-cell capturing

When carrying out the single-cell assay, the single cell was captured on the interface under the inverted microscopy using a pipet by dilution of cell concentration. Fig S2 showed the process of 3 single cells being captured one by one.

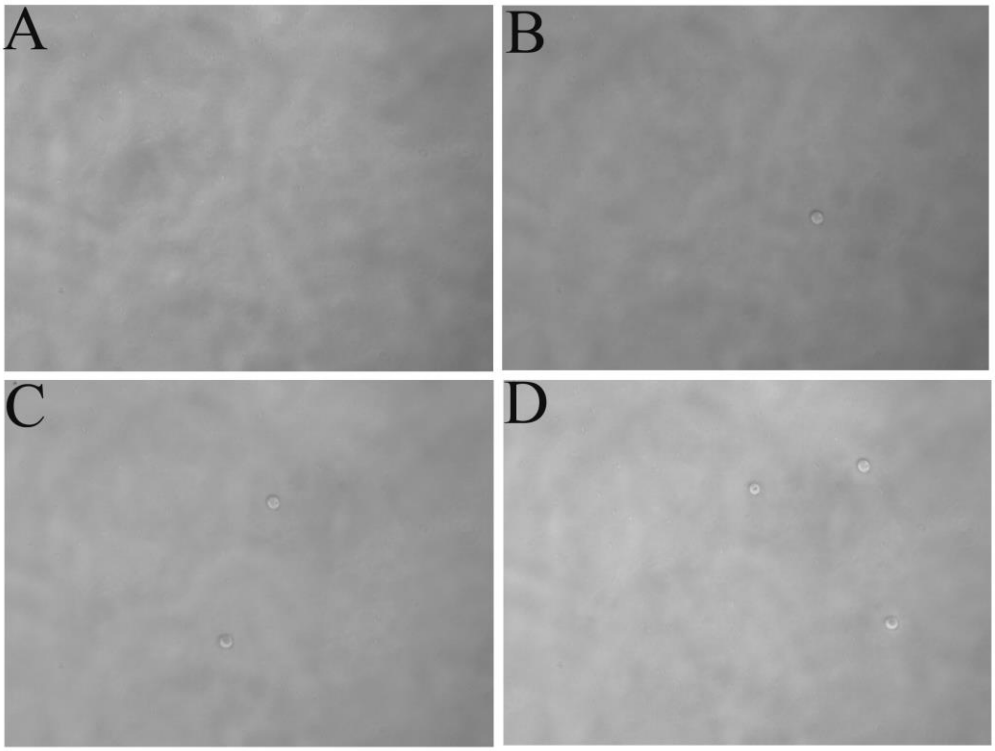

Fig. S2 Inverted microscope images of (A) control, (B) single-cell, (C) 2 cells and (D) 3 cells captured on the interface one by one.

S1.3. Optimization of the concentration of MA-C_{11}

The concentration of MA-C_{11} had an important effect on improving the detection sensitivity of single cell in Fig. S3. As the concentration of MA-C_{11} progressively increased, the ECL signal increased after 0.6 μmol/L and then tended to level off, indicated that the optimum of the concentration of MA-C_{11} was 0.6 μmol/L. These optimal experiment parameters were used in subsequent measurements.

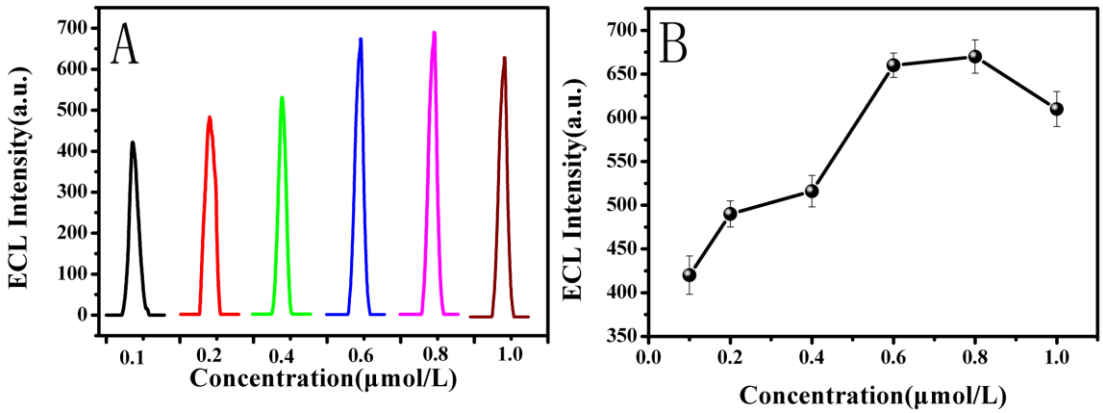

Fig. S3 ECL intensity of MA-C_{11} with different concentration (A) and relationship curves of MA-C_{11} with different concentration (B).

S1.4. Effect of MA-C_n on electronic-transfer rate

As shown in Table S1, the electron-transfer rate decreased as the carbon number in MA-C_n increased because the nonconductive MA with long carbon chain could hinder electron transfer while providing interspace on the electrode surface. The electron-transfer rate test indicated that MA-C_n could to some extent hinder the electron transfer of the sensing interface, which explained why MA-C_{16}-spaced sensor showed inferior performance to the MA-C_{11} counterpart.

Table S1. Effect of MA-C_n on electronic-transfer rate

group	α	k / s^{-1}
FA(MA-C_0)	0.723	0.268
MAA(MA-C_2)	0.472	0.171
MSA(MA-C_4)	0.615	0.127
MHA(MA-C_6)	0.672	0.051
MUA(MA-C_{11})	0.501	0.023
MHDA(MA-C_{16})	0.248	0.017

S1.5. Analytical performance of MUA-spaced single-cell sensor for CD44 receptor

As shown in Fig. S4, the average ECL intensity without MA-C_{11} was calculated to be 387.3 ± 59.2 a.u. ($\bar{x}$ ± s, n = 20) with an RSD of 15.3%. And the average ECL intensity with MA-C_{11} was calculated to be 619.2 ± 61.6 a.u. ($\bar{x}$ ± s, n = 20) with an RSD of 9.9%. The average current intensity was 2.48 ± 0.19 μA ($\bar{x}$ ± s, n = 10, RSD = 7.7%) and 4.03 ± 0.25 μA ($\bar{x}$ ± s, n = 10, RSD = 6.2%) with and without MA-C_{11}, respectively. The results implied the heterogeneity of the single cells as well as the improvement of the accuracy for single-cell analysis.

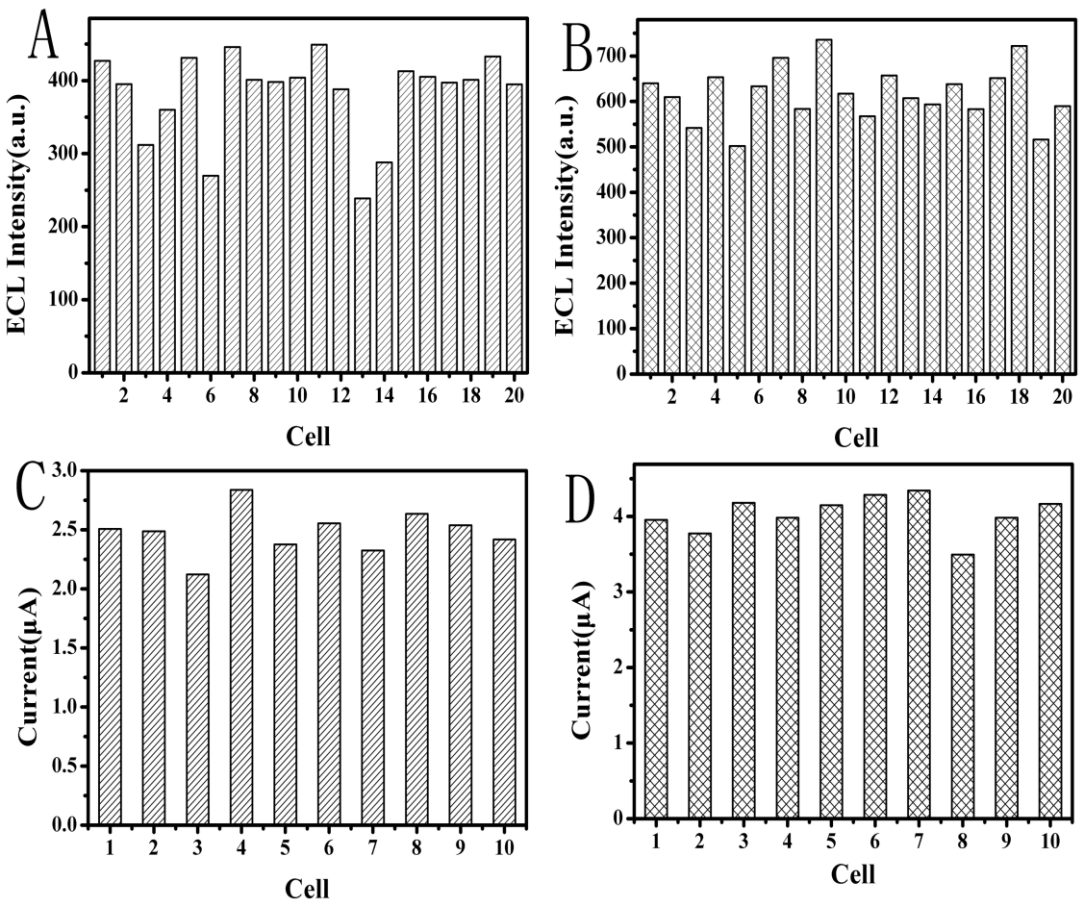

Fig. S4 Histograms of MCF-7 cell capturing without and with MA-C_{11}, respectively by ECL analysis (A, B) and DPV analysis (C, D). Each bar represents one cell.